AIAA JOURNAL
Vol. 34, No. 6, June 1996

Numerical Investigation of Shock Wave Reflections in Steady Flows

J. Vuillon* and D. Zeitoun†
Université de Provence, 13397 Marseille Cedex 20, France
and
G. Ben-Dor‡
Ben-Gurion University of the Negev, Beer Sheva 84105, Israel

To better understand the shock wave reflection phenomenon in steady flows in general, and the transition between regular reflection and Mach reflection in particular, a two-dimensional flowfield model and simulation over a wedge in supersonic flows was investigated. The numerical simulation enabled one to determine the height of the Mach stem in a Mach reflection wave configuration. The determination of the height was pointed out as one of the yet unsolved problems in steady shock wave reflections. The numerical results were compared both with steady flow experiments performed at nominal freestream flow Mach numbers ranging from 2.8 to 5 and with analytical results. Based on the presented numerical investigation, a new geometric parameter that controls the transition between regular reflection and Mach reflection wave configurations was extracted for the flow Mach number range 2.8–7.

Introduction

TWO shock wave reflection configurations are possible in steady flows,[1] namely, regular reflection (RR) and Mach reflection (MR). The RR wave configuration consists of two shock waves: the incident shock wave i and the reflected wave r. These two shock waves intersect at the reflection point R, which is located on the reflecting surface. The MR wave configuration consists of three shock waves: the incident shock wave i, the reflected shock wave r, and the Mach stem m, and one slipstream s. These four discontinuities intersect at a single point called the triple point T located above the reflecting surface. The reflection point R is at the foot of the Mach stem where it touches the reflecting surface. Schematic drawings, as well as the definition of some parameters, of RR and MR wave configurations are shown in Figs. 1a and 1b, respectively.

Consider the MR wave configuration shown in Fig. 2. If one selects a new triple point T^* with its four discontinuities, parallel to those of T, the two triple points T and T^*, as well as all of the other triple points that could have been obtained by choosing a different location for T^* along the incident shock wave i, completely satisfy the conservation equations of the three-shock theory of von Neumann,[2–4] which is the analytical model for describing an MR. Moreover, if experiments conducted with identical initial gasdynamic and geometrical conditions are repeated, then out of the aforementioned infinite theoretically possible MR wave configurations, only one is always obtained. As a consequence, it is pointed out[1,5] that one of the as yet unsolved problems in steady flow shock wave reflections is the way by which the height of the Mach stem of an MR is controlled by the geometrical parameters associated with the reflection phenomenon.

Among the studies concerning these two reflection configurations and in particular the transition between them, i.e., the RR ↔ MR transition, one can cite in particular the experimental works of Henderson and Lozzi,[6,7] Hornung and Kychakoff,[8] and Hornung and Robinson,[9] the numerical work of Auld and Bird,[10] and more recently the one-dimensional analytical approach developed by Azevedo and Liu.[11] In this last paper, the prediction of the Mach stem height of their analytical model showed a trend similar to the experimental results of Ref. 9 but with some discrepancies attributed by Azevedo and Liu to the oversimplified assumptions of their model.

For these reasons, our aim was to focus on the shock wave reflection phenomenon in steady flows, to more precisely study the RR ↔ MR transition. This study was conducted through a numerical simulation of a steady supersonic two-dimensional flowfield between a reflecting wedge and a symmetry line. The steady flow was obtained through the unsteady evolution of an incident flow with a given Mach number M_0. The flowfield was governed by the two-dimensional unsteady Euler equations, which were solved with a finite difference scheme associated with a flux corrected transport (FCT) algorithm. This numerical method, named the LCPFCT method, was developed by Oran and Boris[12] and recently updated by Boris et al.[13]

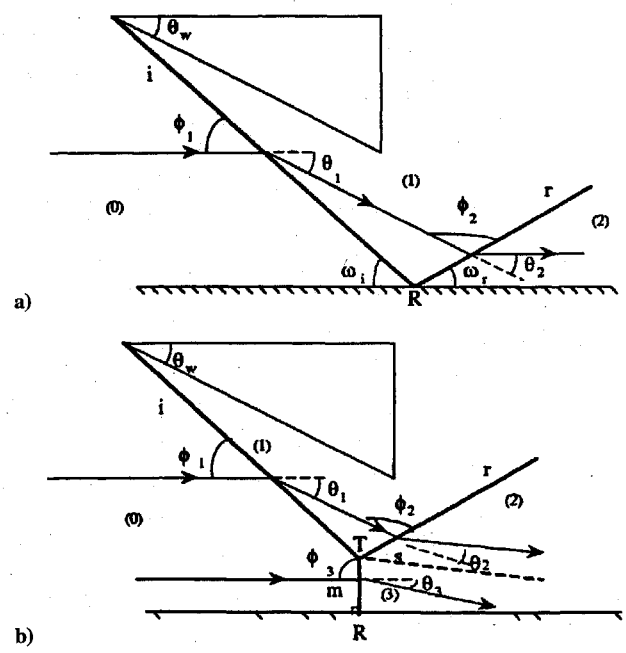

Fig. 1 Schematic illustration of shock wave reflection configurations, and definition of some flow parameters: a) RR and b) MR.

Received Oct. 11, 1994; revision received Jan. 29, 1996; accepted for publication Feb. 16, 1996.

*Graduate Student, Laboratory Institut Universitaire des Systemes Thermiques Industriels (U.M.R CNRS 139), Departement Milieux Hors d'Equilibre, Centre St Jérôme.

†Professor of Fluid Dynamics, Laboratory Institut Universitaire des Systemes Thermiques Industriels (U.M.R CNRS 139), Departement Milieux Hors d'Equilibre, Centre St Jérôme. Senior Member AIAA.

‡Professor of Fluid Mechanics, Pearlstone Center for Aeronautical Engineering Studies, Department of Mechanical Engineering.

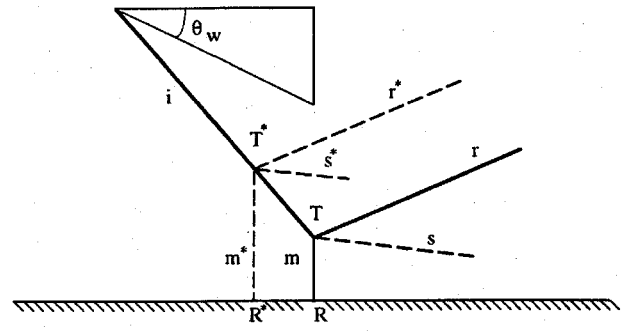

Fig. 2 Schematic illustration of two theoretically possible MR wave configurations for identical initial conditions.

The numerical investigations were performed for different values of the incident flow Mach number M_0 and reflecting wedge angle θ_w, first to validate the computations through comparisons with experimental results,[9] second to compare them with the one-dimensional analytical predictions,[11] and finally to study the influence of the distance between the trailing edge of the reflecting wedge and the symmetry line on the transition. This last point enabled us to extract a new parameter that controls the transition between the RR and MR wave configurations.

Governing Equations

In Cartesian geometry (x, y), the two-dimensional unsteady Euler equations that govern a nondissipative flow can be written in the following generalized conservative form:

$$\frac{\partial \rho}{\partial t} = -\frac{\partial \rho u}{\partial x} - \frac{\partial \rho v}{\partial y} \tag{1}$$

$$\frac{\partial \rho u}{\partial t} = -\frac{\partial (\rho u^2 + P)}{\partial x} - \frac{\partial \rho uv}{\partial y} \tag{2a}$$

$$\frac{\partial \rho v}{\partial t} = -\frac{\partial \rho uv}{\partial x} - \frac{\partial (\rho v^2 + P)}{\partial y} \tag{2b}$$

$$\frac{\partial \rho E}{\partial t} = -\frac{\partial (\rho E + P)u}{\partial x} - \frac{\partial (\rho E + P)v}{\partial y} \tag{3}$$

where u and v are the flow velocity components in the respective x and y directions, P and ρ are the local pressure and density, and E is the total energy per unit mass. To close the system, the perfect gas equation of state is added; it reads

$$P = (\gamma - 1)\rho e \tag{4}$$

where e is the internal energy and γ is the specific heat capacities ratio, i.e., C_p/C_v. The right-hand sides of the preceding set of equations are separated into two parts, the y and the x direction terms. For each of the equations, two equations were obtained by splitting it in each spatial direction; these were solved sequentially by a general one-dimensional continuity equation solver. Details regarding this solver are presented in the next section.

Numerical Method

Integration Stage

The LCPFCT algorithm used in the present study was based on an explicit finite difference scheme associated with a one-dimensional FCT algorithm with fourth-order phase accuracy and minimum residual diffusion. The important properties of FCT are that it is a high-order, monotone, conservative, positivity preserving algorithm. This means that the algorithm is accurate and resolves steep gradients, allowing grid-scale numerical resolution. When a convected quantity, such as density, is initially positive, it remains positive, and no new maxima or minima are introduced resulting from numerical errors in the convection process.[13] This method enables one to solve generalized continuity equations of the form

$$\frac{\partial \phi}{\partial t} = -\frac{1}{r^{\alpha-1}}\frac{\partial (r^{\alpha-1}\phi v)}{\delta r} - \frac{1}{r^{\alpha-1}}\frac{\partial (r^{\alpha-1}D_1)}{\partial r} + C_2\frac{\partial D_2}{\partial r} + D_3 \tag{5}$$

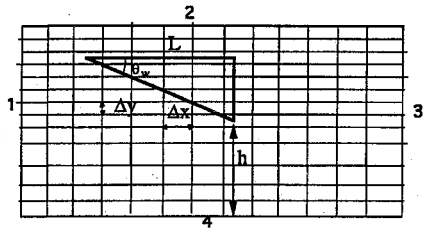

Fig. 3 Schematic illustration of the computational domain implemented around the reflecting wedge and definition of some geometric parameters.

where ϕ is one of the generalized conserved flow quantities, i.e., $(\rho, \rho u, \rho v, \rho E)$, which is transported with the velocity v in the spatial direction r.

For the current problem, $\alpha = 1$ is selected for the resolution in one-dimensional Cartesian geometry. The explicit terms corresponding to C_2, D_1, D_2, and D_3 can be obtained by comparing Eq. (5) to the respective mass [Eq. (1)], momentum [Eqs. (2a) and (2b)], and energy [Eq. (3)] conservation equations.

In each of the integration directions, a time split step approach is used, where the x and y integrations are alternated and each sequential integration constitutes a full convection time step. To carry out these sequential integrations using the split step approach, the time step is chosen such that $\Delta t < 0.4 \min(\Delta t_x, \Delta t_y)$, with Δt_x and Δt_y given by the Courant–Friedrichs–Lewy stability criterion.

Computational Domain and Boundary Conditions

The computational domain is shown in Fig. 3. The flowfield is computed around the reflecting wedge on a Cartesian grid taking into account the reflecting wedge angle θ_w. A first grid was used with a nondimensional spatial step $(\Delta y/L)$ chosen to be equal to 2.310^{-2} and a step $(\Delta x/L)$ adjusted as a function of θ_w as follows: $\Delta x = \Delta y/\tan\theta_w$. The computational domain was meshed around 80 points in the x direction and between 60–110 points in the y direction depending on the investigated distance between the trailing edge of the reflecting wedge and the symmetry line. To prove a grid independent solution at the steady state, a second grid with half-values of the previous spatial steps was also used. The numerical results will be show in the next section.

To avoid prohibitive CPU time, all of the computations were made with the first grid. As a consequence, the time-step integration time, governed by the Courant–Friedrichs–Lewy stability criterion, which depended on the flow fluctuation, had a nondimensional average value of 0.009. About 5000 time-step iterations were required to reach the steady shock wave configuration of the flow around the reflecting wedge. Numerically, this steady flow configuration was considered to be reached when a fourth order of magnitude drop on the L_2 norm residual evolution was obtained. The numerical code ran on an IBM 3090 VF and the CPU time per iteration and grid point was about $7.8\ 10^{-5}$ s/iteration/point.

The boundary conditions of the computational domain (Fig. 3) were as follows.

1) Supersonic inflow conditions were imposed on side 1.

2) Free-slip flow were confined by an insulating hard wall on side 2.

3) Flow parameters were extrapolated in the guard cells to account for the continuity of the flow in the vicinity of the boundary (side 3).

4) The reflection principle was used on the symmetry axis, i.e., side 4.

5) Finally, slip wall conditions were selected on the wedge surface.

These boundary conditions were implemented in the same way as proposed by Boris et al.[13] It consisted of developing extrapolations from the interior computational domain to guard boundary cells outside of this domain. These guard boundary cells allow cells on the domain boundary to be treated as interior cells.

Results and Discussion

Code Validation

In Fig. 1, the flow behind the incident shock wave, in state 1 is supersonic $(M_1 > 1)$. Thus, in state 1, a situation in which a supersonic

flow is directed toward the symmetry line is obtained, and this flow must negotiate a fictitious wedge with an angle θ_w. Two cases are possible, functions of the maximum flow deflection angle $\delta_{max}(M_1)$ (Ref. 14): 1) if $\theta_w < \delta_{max}(M_1)$, the flow can become parallel to the symmetry line through an attached shock wave, which emerges from the reflection point R, and results in a RR wave configuration, (see Fig. 1a); and 2) if $\theta_w > \delta_{max}(M_1)$, the flow will be deflected away from the symmetry line by a detached shock wave, which leads to a MR wave configuration, (see Fig. 1b). These flow configurations have been used to validate the numerical approach of the present study, and three different pairs of M_0 and θ_w values were tested.

Detached Shock Wave

An incident flow Mach number $M_0 = 2.84$ and a reflecting wedge angle $\theta_w = 40$ deg were first chosen. This large reflecting wedge angle is greater than the analytical maximum flow deflection angle $\delta_{max}(M_0)$, which for $M_0 = 2.84$ is equal to 33 deg. Thus, the conditions of the selected numerical simulation are far from the detachment value, and one should expect a detached shock wave ahead of the reflecting wedge.

The flow Mach number distribution, which was obtained when the steady-state solution was reached, is shown in Fig. 4. The detached shock wave causes the flow in front of the leading edge of the reflecting wedge to become subsonic and to negotiate the wedge surface through a continuous subsonic turning.[1,14] The sonic line clearly defines two subsonic zones: one located to the front of the reflecting wedge just behind the detached shock wave and one behind the trailing edge of the reflecting wedge. Along the stagnation streamline the flow Mach number drops from $M_0 = 2.84$ to a subsonic value $M_1 = 0.49$ just behind the straight part of shock wave front. This value agrees well with the theoretical value, which yields 0.485. Based on the foregoing discussion it could be concluded that the first numerical simulation of the evolution of the two-dimensional inviscid flowfield around the reflecting wedge correctly described the detached shock wave configuration.

For all of the other numerical simulations, the reflecting wedge angle θ_w was chosen to be smaller than the maximum deflection angle $\delta_{max}(M_0)$ to ensure that an attached oblique shock will be generated at the leading edge of the reflecting wedge.

RR Wave Configuration

To study an RR wave configuration of an oblique shock wave, a numerical experiment with a flow Mach number $M_0 = 2.84$ and a reflecting wedge angle $\theta_w = 17.5$ deg was conducted. The ratio h/L was set to be equal to 0.37. Here h is the distance between the trailing edge of the reflecting wedge and the symmetry line, and L is the length of the reflecting wedge (see Fig. 3).

Figure 5 represents the distribution of the Mach number isolines around the reflecting wedge when the steady state is reached in the

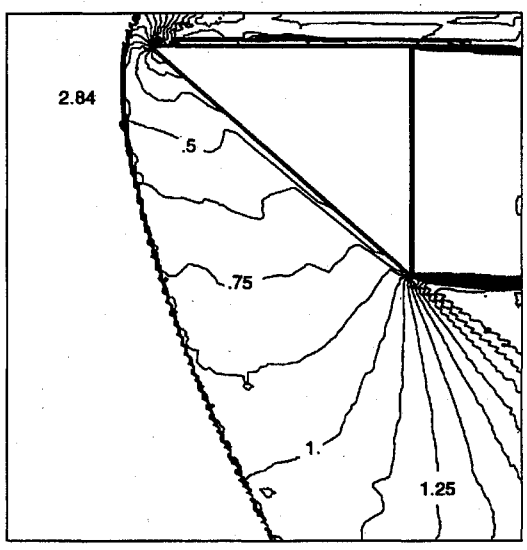

Fig. 4 Mach number distribution of a steady detached shock wave obtained for $M_0 = 2.84$ and $\theta_w = 40$ deg.

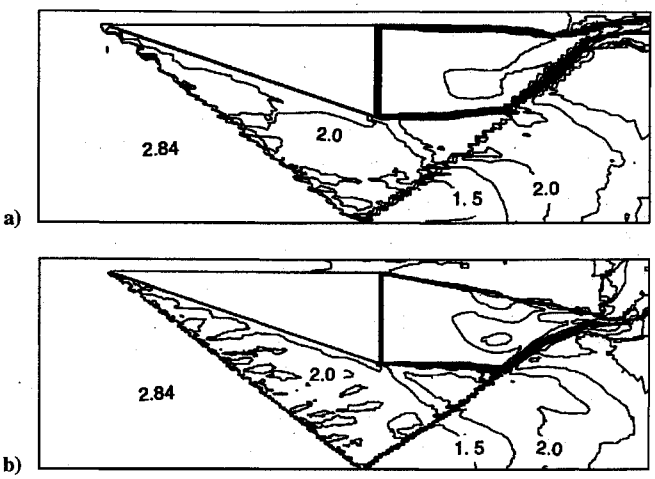

Fig. 5 Mach number isolines of the steady-state RR wave configuration for $M_0 = 2.84$, $\theta_w = 17.5$ deg, and $h/L = 0.37$.

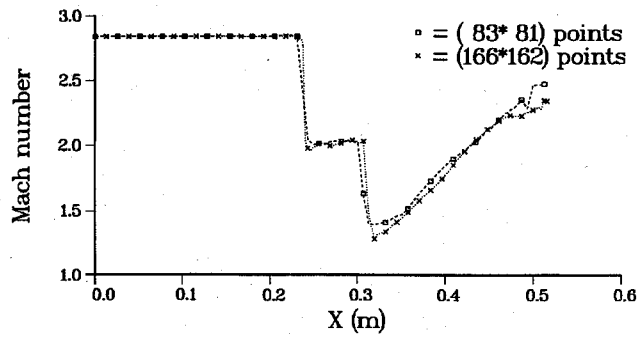

Fig. 6 Mach number distribution along a longitudinal line located at $h/3$ for $M_0 = 2.84$, $\theta_w = 17.5$ deg, and $h/L = 0.37$.

two mesh configurations just described: Fig. 5a coarse mesh, Fig. 5b finer mesh. One can see a quasi-identical shock wave structure with the same position of the reflecting point on the symmetry axis and of relating incident and reflected shock waves angles i and r, which corresponds to an RR. There, respective wave angles $\omega_i = 35$ deg and $\omega_r = 28.5$ deg indicate that the RR is a nonspecular reflection. Notice also the subsonic zone behind the reflecting wedge and the interaction of the reflected shock wave with the leading expansive wave of the expansion fan, which is developed at the trailing edge of the reflecting wedge.

Figure 6 represents the flow Mach number distribution along a longitudinal line located at $h/3$ from the symmetry axis, for the two mesh configurations. These curves are quasi-identical, and the slope of the shock waves was obviously better described in the finer grid. The first drop in the flow Mach number is a result of the incident shock wave i. The drop is from $M_0 = 2.84$ to $M_1 = 2.0$. The second drop is a result of the reflected shock wave r behind which one gets $M_2 = 1.41$. The analytical angle of incidence and flow Mach number are $\phi_1 = 36.15$ deg and $M_1 = 2.01$, respectively. State 1, behind the incident shock wave i with $M_1 = 2.01$ and $\theta_w = 17.5$ deg also corresponds to the case where $\theta_w < \delta_{max}(M_1)$, and hence an RR can be obtained for these initial conditions. The discrepancy between the incident shock wave angle ϕ_1 as calculated numerically and analytically is less than 1%. These comparisons allowed the use of the first mesh to continue this study with a reduced CPU time.

MR Wave Configuration

Finally, the model of the MR wave configuration of an oblique shock wave was carried out with $M_0 = 3.49$, $\theta_w = 23$ deg, and $h/L = 0.37$. These values of M_0 and θ_w correspond to a point in the dual domain in which the two shock wave configurations RR and MR theoretically exist. Recently, experimental and numerical works[15,16] have confirmed this theory and have shown that these two stable configurations can be obtained through an hysteresis cycle.

From a constant initial computational plane, given by the upstream flow conditions, the first obtained steady state is an RR configuration, as shown Fig. 7b. This solution is stable. To avoid describing the hysteresis cycle, by increasing the wedge angle until the detachment criteria were reached and later decreasing this wedge angle until the value of θ_w to obtain the MR transition, it is possible to accelerate its transition to an MR wave configuration by introducing, during a time step, a small pressure disturbance behind the reflected shock wave.[17] This disturbance, in addition to the large streamline deflection angle imposed on the symmetry line, resulted in an MR wave configuration. The triple point moved along the incident shock wave i (see Figs. 5c–5e) until a steady-state solution configuration of the flowfield was finally reached (see Fig. 7f).

Figure 8 shows the steady-state solution obtained through the flow Mach number distribution. An MR wave configuration consisting of three shock waves is clearly visible: the incident shock wave i, for which $\phi_1 = 38$ deg; the reflected shock wave r, for which $\phi_2 = 25.5$ deg; and the Mach stem m, which is seen to be perpendicular to the symmetry line. Because of the relative thickness of the grid steps, the Mach stem is seen to be straight. As will be shown in the next section, this numerical observation enables us to obtain the Mach stem height with an accuracy equal to the vertical spatial step, which has the same order of magnitude as the curvature in the vicinity of the triple point.[1] The slipstream separating the subsonic region 3 behind the Mach stem m and the supersonic region 2 behind the reflected shock wave r is also clearly visible in Fig. 8. The sonic line in region 3, which is added to the MR wave configuration in Fig. 8, clearly defines the subsonic flow zone behind the Mach stem. The sonic line is seen to follow the slipstream until it breaks away from it and terminates on the symmetry line. The point where the sonic line breaks away from the slipstream defines, in fact, the location of the throat of the converging nozzle formed by the slipstream and the symmetry line. Because of the weak transversal velocity gradients, the sonic line is quite perpendicular to the symmetry line in the vicinity of this throat. The numerical simulation, shown in Fig. 8, contradicts Azevedo and Liu's[11] main assumption that the throat of the aforementioned converging nozzle is located at the point where the leading characteristic of the expansion fan formed at the trailing edge of the reflecting wedge intersects the slipstream. The Mach angle μ_1, which can be calculated from the numerical value of the Mach number $M_1 = 2.1$, is equal to 28.5 deg and is shown in Fig. 8. One can clearly see that the sonic throat is not located at the point of intersection between the leading characteristic of the expansion fan and the slipstream. This point of intersection is seen in Fig. 8 to be ahead of the actual throat.

The numerical flow Mach number distribution along the symmetry line is shown in Fig. 9. One can see the flow Mach number drop from $M_0 = 3.49$ to $M_3 = 0.4$ becaue of the Mach stem. Then the flow Mach number is seen to increase linearly behind the Mach stem to 1 at the sonic line, which is located 0.265 m from the left boundary. The foregoing described simulation revealed that although Azevedo and Liu[11] were correct in assuming that the slipstream and the symmetry line form a one-dimensional converging nozzle, they were wrong in determining the location of the throat of the converging nozzle.

Based on these comparisons between the numerical simulations of a detached shock wave, an RR and an MR and their analytical solutions, it could be concluded that the code developed is capable of

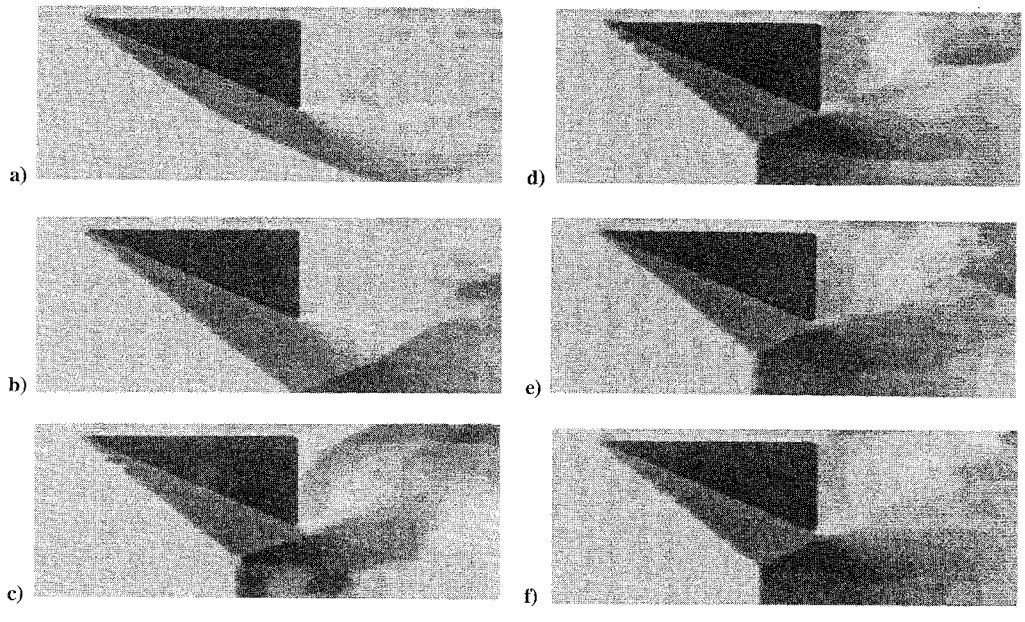

Fig. 7 Density flowfield evolution from the initial conditions to the steady-state MR for $M_0 = 3.49$, $\theta_w = 23$ deg, and $h/L = 0.37$.

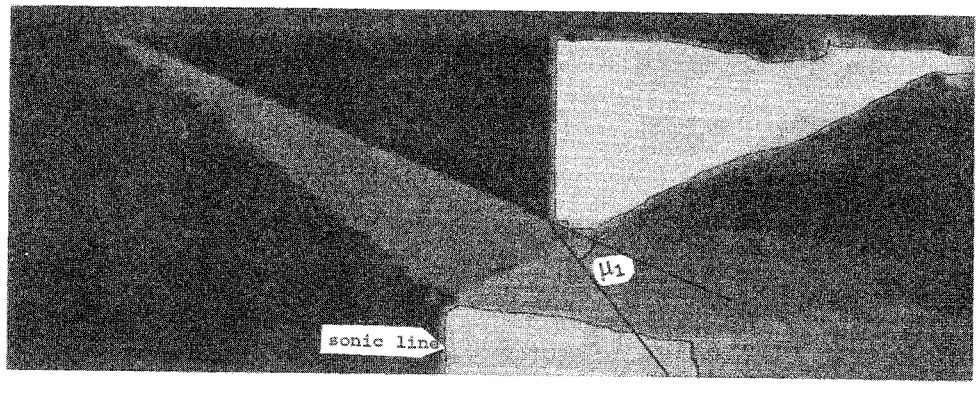

Fig. 8 Mach number flowfield of the steady-state MR wave configuration shown in Fig. 7f.

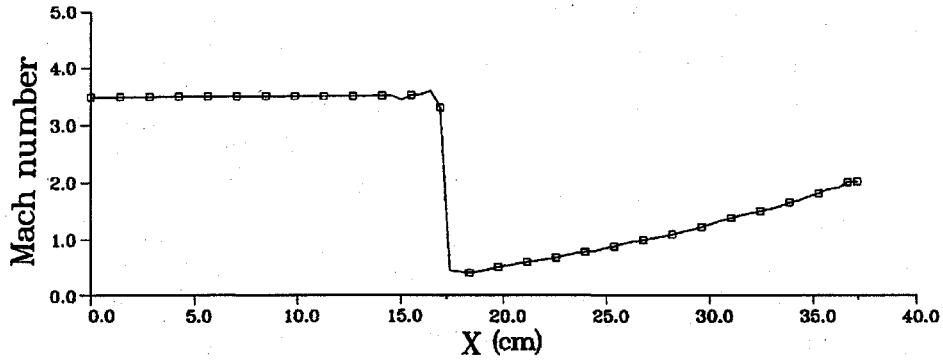

Fig. 9 Mach number distribution along a longitudinal line located at $h/3$ for $M_0 = 3.49$, $\theta_w = 23$ deg, and $h/L = 0.37$.

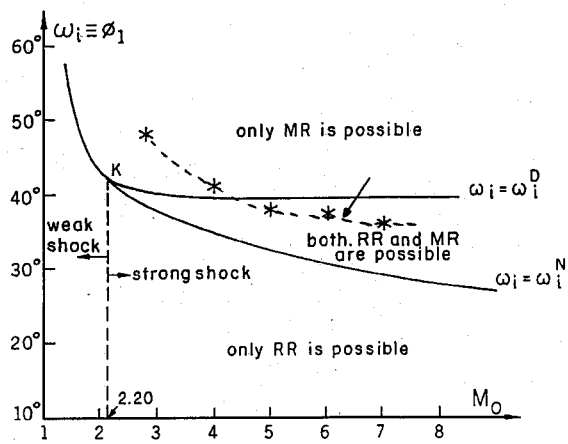

Fig. 10 Domains of different types of reflections in the (M_0, ω_i)-plane for $\gamma = 1.4$ and $h/L = 0.37$.

Table 1 Upstream conditions of the various numerical simulations

M_0	T_0, K	P_0, MPa
2.84	300	0.31
3.49	300	0.49
3.98	300	0.76
4.96	365	1.54

Table 2 Incident reflecting wedge angles for the various numerical simulations

M_0	2.84	3.98	4.96
θ_w, deg	19	22	22
—	21	23	23
—	—	—	25
—	—	—	26.56

well simulating these flowfields. Consequently, in the next section, the MR wave configuration will be more precisely studied to predict the Mach stem height L_m and to compare it with existing analytical and experimental data.

Prediction of the Height of the Mach Stem

Position of the Problem

Graphical solutions in the pressure deflection plane (P, θ) traditionally have been used to better understand the transition between RR and MR[1] wave configurations. The shock polar presentation led to two RR $\leftrightarrow$ MR transition criteria. The transition lines corresponding to these transition criteria are shown in Fig. 10 in the (M_0, ω_i) plane for fixed values of h/L and γ. The detachment $\omega_i = \omega_i^D$ and the von Neumann $\omega_i = \omega_i^N$ criteria[1-4] divide the (M_0, ω_i) plane in to three domains: 1) a domain in which only RR wave configurations are theoretically possible, $\omega_i < \omega_i^N$; 2) a domain in which only MR wave configurations are theoretically possible, $\omega_i > \omega_i^D$; and 3) the dual domain, $\omega_i^N < \omega_i < \omega_i^D$, in which both RR and MR wave configurations are theoretically possible.

Until recently Hornung and Robinson's[9] experimental results were accepted in the scientific community as the state of art concerning the RR $\leftrightarrow$ MR transition in steady flows. Based on their experiments, as well as those of Henderson and Lozzi[6,7] and Hornung and Kychakoff,[8] the conclusion was that in steady flows with $M_0 > 2.20$ the transition from regular to MR occurs at the von Neumann condition $\omega_i = \omega_i^N$. As a consequence, it was accepted that only MR wave configurations can exist inside the dual domain. This conclusion recently has been refuted, and it was shown the existing stable RR and MR configurations[15,16] in the dual domain in the range $\omega_i^N < \omega_i < \omega_i^D$.

The next part of the study is aimed at numerically extracting the Mach stem height, for various initial values $(M_0, \theta_w, h/L)$ to show the transition between the RR and MR wave configurations.

Numerical Results

To compare the computations with experimental results, four different upstream conditions were chosen from the experiments conducted by Hornung and Robinson.[9] These conditions are given in Table 1. Note that for these experimental conditions, the flowfield depends only on the incident flow Mach number M_0.

Since all of the experiments were carried out with $h/L = 0.37$, the geometrical setup of the experiment was fixed through this ratio, and the numerical solution was implemented for various reflecting wedge angles θ_w. These reflecting wedge angles are listed in Table 2. Based on the foregoing discussion on the transition lines between the RR and MR wave configurations, Hornung and Robinson's experiments[9] were conducted inside the dual domain to predict the transition angle and the Mach stem height corresponding to the MR solution. It should also be noted that in the two-dimensional numerical results the accuracy in the prediction of the wave reflection phenomenon is equal to the nondimensional vertical space steps, and for all of the numerical experiments conducted in this case, this accuracy was under 1%. This allowed an accurate prediction of the steady-state flowfield solution, and this numerical approach easily could complete the available data on the MR wave configuration.

Figure 11, which is a reproduction from Ref. 11, contains Hornung and Robinson's[9] data and the analytical results of Azevedo and Liu.[11] The numerical results of the present study are added to this figure. Notice that the present results, obtained for $M_0 = 2.84$, 3.98, and 4.96, are in full agreement with the experimental ones. However, the one-dimensional analytical model suggested by Azevedo and Liu[11] gives a similar trend but underpredicts the experimental results. This is because of the oversimplifying assumptions that were implied in their one-dimensional model. Note that, in general (Fig. 1b), the deflected streamlines behind the Mach stem are usually directed toward the symmetry line $\theta_0 \neq 0$ and, hence, the velocity can no longer be considered parallel to the symmetry line. This is clearly shown in the Mach number distribution shown in Fig. 8, where transversal velocity gradients are seen to exist in the subsonic region 3 immediately behind the Mach stem. As a consequence, this region can only be assumed to be one dimensional in the vicinity of the throat. In addition, as mentioned earlier, the numerical experiments reject the second assumption of their model, that the leading characteristic of the expansion fan, originating at the

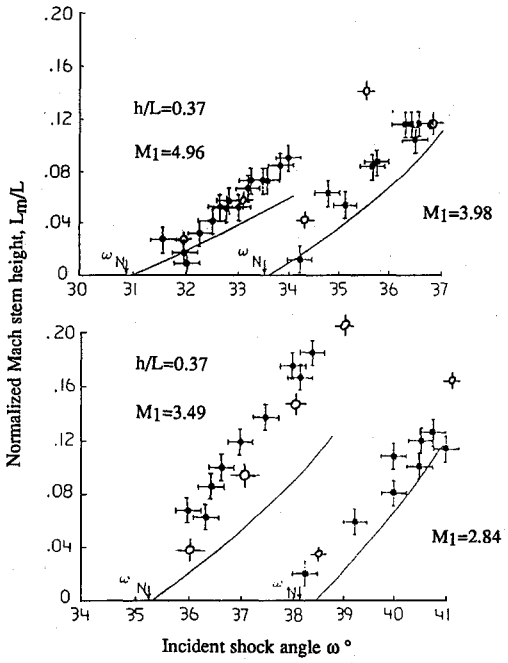

Fig. 11 Analytical and numerical predictions of the Mach stem height, L_m, and comparison with experimental results: •, Hornung and Robinson data[9]; ——, inviscid theory[11]; and ○, two-dimensional inviscid numerical results.

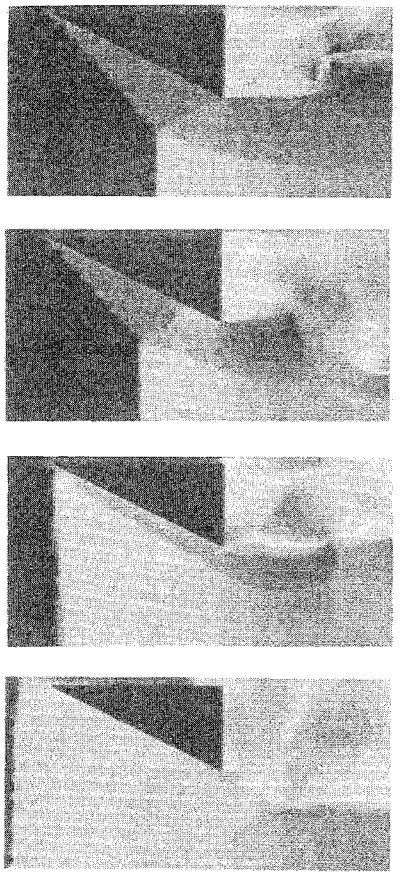

Fig. 12 Mach number flowfield evolution of the transient process between an unstable MR wave configuration and a detached shock wave in front of the reflecting wedge for $M_0 = 2.84$, $\theta_w = 26.5$ deg, and $h/L = 0.37$.

trailing edge of the reflecting wedge and refracted by the reflected shock wave, intersects the slipstream s and defines the location of the sonic throat in the region behind the Mach stem m.

The numerical results obtained for $M_0 = 3.49$ are also plotted in Fig. 11. One can see that they underestimate the experimental values. Furthermore, an extrapolation of the experimental data seems to give a transition angle corresponding to the von Neumann criterion, equal to $\omega^N = 34.5$ deg, inferior to the analytical and numerical one of $\omega^N = 35.3$ deg. In this particular case, Hornung and Robinson's experimental results[9] were most likely dominated by downstream influence which led to a lower transition angle. This phenomenon, which was reported by Azevedo,[18] discards the reliability of the experimental results for $M_0 = 3.49$.

Finally, it is evident from Fig. 11 that the analytical, the experimental, and the numerical predictions of the Mach stem height as a function of the incident shock wave angle ω_i depend on the geometrical setup determined by the ratio $h/L = 0.37$. As a consequence of this fixed value, one can see that the Mach stem height never exceeds the value $L_m/L = 0.22$. The upper limiting situation corresponds to the case where the reflected wave r grazes the trailing edge of the reflecting wedge. For example, in Fig. 8, if the reflecting wedge angle is increased by 1 deg, then the MR becomes unstable and its Mach stem moves upstream until the MR vanishes and a bow shock wave is established ahead of the leading edge of the reflecting wedge. This transient process is illustrated in Fig. 12 with the formation of a secondary MR over the reflecting wedge surface, as the triple point moves upstream along the incident shock wave i. Finally, a detached bow shock wave is obtained in front of the reflecting wedge. The flow in the converging nozzle, formed by the surface of the reflecting wedge and the symmetry line, becomes subsonic and the nozzle is said to be unstarted. It is important to note that this detached bow shock wave was obtained for a wedge angle $\theta_w = 26.5$ deg, which was smaller than the maximum flow deflection angle $\delta_{\max}(M_0)$, which for $M_0 = 2.84$ is equal to 33 deg. As a consequence, there are no doubts that this detached bow shock wave arises only from the geometric length scales w, L, and h.

Thus, for a geometrical setup fixed through the ratio $h/L = 0.37$, the Mach stem is limited both by the lower limit arising from the von Neumann criterion ω_i^N and by the upper limit arising from the detached shock wave configuration obtained when the nozzle is unstarted. For fixed values of M_0 and h/L it is possible to extract a similar detachment angle $\omega_i = \omega_i^u$, corresponding to the case where the nozzle is unstarted. Note that the narrow domain corresponding to the range $\omega_i^N < \omega_i < \omega_i^u$ finally leads to a linear evolution of the normalized Mach stem height L_m/L as a function of the incident shock wave angle.

The limiting situation corresponding to the case where the reflected wave r arising from the triple point T grazes the trailing edge of the reflecting wedge also corresponds to the lower distance $h_{\min}$ between the symmetry line and the reflecting wedge. Whenever the distance h is reduced below $h_{\min}$ (i.e., whenever $h < h_{\min}$), the two-dimensional nozzle is unstarted.

In this approach, the direction of investigation is more particularly focused on the evolution of the different wave configurations as a function of the distance h for a fixed reflecting wedge angle value θ_w.

These numerical investigations presented in the next section enable us to extract a new parameter affecting the transition between RR and MR wave configurations in steady flows.

Dependence of the RR ↔ MR Transition on the Distance h

As already described, the wave reflection configuration strongly depends on the length scales h, L, and w associated with the reflecting wedge angle θ_w. Consequently, to study the influence of the geometry on the reflection phenomenon, numerical simulations were carried out for several values of h/L, starting from an isoincidence line of the (M_0, ω_i) plane. In the present case, numerical experiments were conducted with the isoincidence $\theta_w = 26.56$ deg, shown in Fig. 10.

Note that since the geometry is two dimensional, the distance h between the symmetry line and the trailing edge of the reflecting wedge represents an exit area per unit depth. In addition, for a given set of values of M_0, θ_w, and L, either RR or MR wave configurations could take place, provided that $h_{\min} < h < h_{\max}$. The lower value, $h_{\min}$, between the trailing edge of the reflecting wedge and the symmetry line corresponds to the limiting situation described earlier in which the nozzle becomes unstarted. The upper value, $h_{\max}$, is the distance

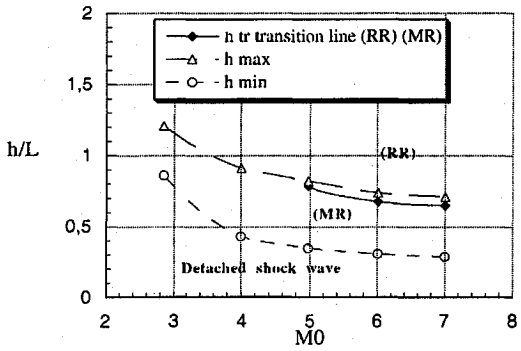

Fig. 13 Dependence of h_{min}, h_{max}, and h_{tr} on the incident flow Mach number M_0 for $\theta_w = 26.56$ deg.

between the trailing edge of the reflecting wedge and the point where the leading characteristic of the expansion fan emanating from the trailing edge of the reflecting wedge intersects the incident shock wave i. For a value $h > h_{max}$, whenever an MR is obtained, the actual incident shock wave is weaker than the one emanating from the leading edge of the reflecting wedge because of the interaction of the expansion fan with the incident shock wave. To more precisely extract the exact distance h_{tr} where the transition between the RR and MR wave configurations took place, several numerical simulations were conducted for the flow Mach number range $2.84 < M_0 < 7$ with a fixed wedge angle $\theta_w = 26.56$ deg. The characteristic values h_{min}, h_{max}, and h_{tr} deduced graphically for each simulation are plotted in Fig. 13. The following comments are self-explanatory.

1) If $h < h_{min}$, the converging nozzle is said to be unstarted and a detached bow shock wave is formed ahead of the reflecting wedge.

2) If $h_{min} < h < h_{tr}$, an MR wave configuration is established inside the converging nozzle.

3) If $h_{tr} < h < h_{max}$, an RR wave configuration is established inside the converging nozzle.

The point where the transition h_{tr} line intersects the h_{max} line results in the limiting situation where the leading expansion fan intersects the incident shock wave i. In this case, whenever an MR configuration is obtained for $h > h_{max}$, the incident shock wave in the vicinity of the symmetry line is no longer identical to the one formed at the leading edge of the reflecting wedge.

Note that for all of the numerical experiments conducted in the range $h_{min} < h < h_{tr}$, the obtained RR wave configurations were not kept and pressure disturbances were introduced behind their reflected shock waves to give rise to MR wave configurations if they exist.[17]

Conclusion

The interaction of an inviscid two-dimensional supersonic flow with a reflecting wedge, situated above a symmetry line, was numerically studied. The governing Euler equations were solved by an explicit finite difference scheme, LCPFCT, which belongs to the more general FCT methods. The computational domain was meshed with a Cartesian grid by fitting the reflecting wedge angle θ_w with the spatial steps in each direction. This method was particularly convenient in the present case and allowed very low CPU times because it avoided the need to express the Euler equations in generalized coordinates.

The flowfield model was validated through comparisons with analytical values to point out the different flow configurations resulting from the interaction of a supersonic flow with a reflecting wedge. These wave configurations were either an RR, an MR, or a detached bow shock wave in front of the leading edge of the reflecting wedge.

The numerical code was found to successfully predict the Mach stem height of an MR configuration out of the infinite possible ones deduced from the three shock theory. The two-dimensional numerical results were found to agree with the experimental results and enabled us to obtain greater accuracy in the prediction of the Mach stem height than the only available analytical one-dimensional model.

It has been shown that the flowfield established inside the converging nozzle depends not only on the gasdynamic conditions M_0 and θ_w, but also on geometrical parameters, e.g., the distance between the trailing edge of the reflecting wedge and the symmetry line h.

For a given set of gasdynamic initial conditions, i.e., incident flow Mach number M_0 and reflecting wedge angle θ_w, there are three critical values of the distance from the trailing edge of the reflecting wedge to the symmetry line, namely, h_{min}, h_{tr}, and h_{max}. This finding is very important if one is to design converging nozzles such as in engine intakes.

For $h < h_{min}$ the converging nozzle is unstarted and a bow shock wave is formed ahead of the leading edge of the reflecting wedge, even if the reflecting wedge angle θ_w is smaller than the detachment angle corresponding to M_0, i.e., $\theta_w < \delta_{max}(M)$; for $h_{min} < h < h_{tr}$ an MR is formed inside the converging nozzle; for $h_{tr} < h < h_{max}$ an RR is formed inside the converging nozzle. For $h > h_{max}$ the gasdynamic initial conditions change as the expansion fan emanating from the trailing edge of the reflecting wedge interacts with the incident shock wave emanating from the leading edge of the reflecting wedge, and changes its nature.

As a final remark note that the present numerical work enables one to complete the available experimental data on the steady shock wave reflection phenomenon. In future work, real gas effects will also be taken into account to extend the study to the hypersonic Mach number range.

Acknowledgment

The authors would like to thank the Centre de Calcul de St Jérôme for allowing access to the IBM 3090 VF.

References

[1]Ben-Dor, G., *Shock Wave Reflection Phenomena*, Springer–Verlag, New York, 1991.

[2]Von-Neumann, J., "Oblique Reflection of Shock," Bureau of Ordinance, Explosives Research Rept. 12, Navy Dept., Washington, DC, 1943.

[3]Von-Neumann J., *Collected Works*, Vol. 6, Pergamon, Oxford, England, UK, pp. 238–299.

[4]Von-Neumann, J., "Refraction, Intersection and Reflection of Shock Waves," Bureau of Ordinance, Navy Dept., NAVORD Rept. 203-45, Washington, DC, 1945.

[5]Ben-Dor, G., and Takayama, K., "The Phenomena of Shock Wave Reflection—A Review of Unsolved Problems and Future Research Needs," *Shock Waves*, Vol. 2, No. 4, 1992, pp. 211–223.

[6]Henderson, L. F., and Lozzi, A., "Experiments on Transition of Mach Reflection," *Journal of Fluid Mechanics*, Vol. 68, Pt. 1, 1975, pp. 139–155.

[7]Henderson, L. F., and Lozzi, A., "Further Experiments on Transition of Mach Reflection," *Journal of Fluid Mechanics*, Vol. 94, Pt. 3, 1979, pp. 541–539.

[8]Hornung, H. G., and Kychakoff, G., "Transition from Regular to Mach Reflection of Shock Waves in Relaxing Gases," *Proceedings of the 11th International Symposium on Shock Tubes and Waves* (Seattle, WA), edited by B. Ahlborn, A. Hertzberg, and D. Russel, Univ. of Washington Press, 1977, pp. 292–302.

[9]Hornung, H. G., and Robinson, M. L., "Transition from Regular to Mach Reflection of Shock Waves, Part 2. The Steady-Flow Criterion," *Journal of Fluid Mechanics*, Vol. 123, 1982, pp. 155–164.

[10]Auld, D. J., and Bird, G. A., "The Transition from Regular to Mach Reflection," AIAA Paper 76-322, July 1976.

[11]Azevedo, D. J., and Liu, S. L., "Engineering Approach to the Prediction of Shock Patterns in Bounded High-Speed Flows," *AIAA Journal*, Vol. 31, No. 1, 1993, pp. 83–90.

[12]Oran, E. S., and Boris, J. P., *Numerical Simulation of Reactive Flow*, Elsevier, New York, 1987.

[13]Boris, J. P., Landsberg, A. M., Oran, E. S., and Gardner, J. H., "LCPFCT-A Flux Corrected Transport Algorithm for Solving Generalized Continuity Equations," Lab. for Computational Physics and Fluid Dynamics, Naval Research Lab. Rept. NRL/MR/6610-93-7192, April 1993.

[14]Liepmann, H. W., and Roshko, A., *Elements of Gasdynamics*, Wiley, New York, 1957, pp. 85–123.

[15]Choupn, A., Passerel, D., Li, H., and BenDor, G., "Reconsideration of Oblique Shock Wave Reflections in Steady Flows. Part 1: Experimental Investigation," *Journal of Fluid Mechanics*, Vol. 301, 1995, pp. 19–35.

[16]Vuillon, J., Zeitoun, D., and Ben-Dor, G., "Numerical Investigation on the Prediction of the Mach Stem in Steady Flows," International Symposium of Shock Waves, Pasadena, CA, Paper 78, July 1995.

[17]Vuillon, J., "Modélisation et simulation numérique des écoulements confinés Eulériens instationnaires," Ph.D. Thesis, Dept. Milieux Hors d'Equilibre, Université de Provence, Marseille, France, July 1994.

[18]Azevedo, D. J., "Analytical Prediction of Shock Patterns in a High-Speed Wedge Bounded Duct," Ph.D. Thesis, Dept. of Mechanical and Aerospace Engineering, State Univ. of New York, Buffalo, NY, June 1989.